



The normal state Hall effect in $\text{Nd}_{1-2x}\text{Ca}_x\text{M}_x\text{Ba}_2\text{Cu}_3\text{O}_{7-\delta}$ (M = Pr, Th): Evidence for hole localization by disorder

S.R. Ghorbani^{a,*}, M. Andersson^b, Ö. Rapp^b

^a Department of Physics, Tarbiat Moallem University of Sabzevar, P.O. Box 397, Sabzevar, Iran

^b Solid State Physics, Department of Microelectronics and Information Technology, KTH Electrum 229, SE-164 40 Kista, Sweden

Received 31 October 2004; received in revised form 10 May 2005; accepted 10 May 2005

Available online 29 June 2005

Abstract

The transport properties of sintered samples of $\text{Nd}_{1-2x}\text{Ca}_x\text{M}_x\text{Ba}_2\text{Cu}_3\text{O}_{7-\delta}$ (M = Pr, Th) with $0 \leq x \leq 0.10$ have been studied in the normal state by Hall effect measurements. The Hall coefficient at high temperature was almost constant for Ca–Pr while it increased with increasing Ca–Th doping concentration. The results for the Hall coefficient as a function of temperature and doping concentration were analyzed within two different models. A good agreement between models and data was obtained. On the basis of these models, it was inferred that Ca–Pr and Ca–Th doping introduce electronic disorder in the CuO_2 planes. The localization tendency is driven by electronic disorder. This is the main reason for strong depression of the superconducting critical temperature in both alloys. It was found that the Hall angle is proportional to T^2 in the whole measured temperature range in Ca–Pr doped samples while there are deviations at high temperature in the Ca–Th doped series. In a phenomenological narrow band model, the conduction band was asymmetric for the pure sample and this asymmetry decreased with increasing Ca–Th doping while it was almost constant for Ca–Pr doped samples.

© 2005 Elsevier B.V. All rights reserved.

PACS: 74.72.Jt; 74.25.Fy

Keywords: Nd-123; Charge neutral doping; Hall effect; Localization

1. Introduction

The often strong dependence of the superconducting critical temperature T_c on doping in high- T_c superconductors can be empirically described

* Corresponding author. Tel.: +98 9155712461; fax: +98 5714411161.

E-mail address: ghorbani@sttu.ac.ir (S.R. Ghorbani).

by the well known relation between T_c and hole density, p , in the CuO_2 planes. The maximal T_c is found at $p \approx 0.16$ with a parabolic decrease of T_c for larger and smaller p , and destruction of superconductivity when p is varied by more than ± 0.1 from its optimal value [1]. This model has a remarkably general validity for charge doped high- T_c s. Therefore it is a challenging observation that T_c in some charge neutrally doped alloys is similarly strongly depressed. In $\text{RE}_{1-2x}\text{Ca}_x\text{M}_x\text{Ba}_2\text{Cu}_3\text{O}_{7-\delta}$ with $\text{RE} = \text{Y}, \text{Sm}, \text{Gd}, \text{Nd}$, and $\text{M} = \text{Th}$ or Pr , and for $x \leq 0.1$ where Pr is +4 valent, the charge concentration is constant for Ca–Th or Ca–Pr doping [2–7]. Yet the observed depression of T_c , now linear instead of parabolic, has a slope $-dT_c/dx$ in the range 150–230 K.

In the efforts to understand the effect of Pr when doped alone into 123 compounds, it was early noted that a charge filling picture is incomplete [2,8,9]. Other mechanisms suggested for this controversial problem include pair breaking due to the Pr magnetic moment, hole localization, and hybridization of the Pr with electrons in the CuO_2 plane. Recently we found evidence from neutron diffraction and bond valence sum calculations in Nd(Pr) doped 123, that up to $x \approx 0.1$ the depression of T_c is due to both hole filling and charge localization [10]. At larger dopings the hole filling mechanism is arrested by the apparent valence shift of Pr to +3, while an increasing localization on RE site persists all the way up to close to the disappearance of superconductivity.

Notwithstanding the similar depression of T_c for $(\text{Ca-Pr})_x$ and $(\text{Ca-Th})_x$ doped 123 compounds, there are noteworthy differences between the electronic properties for these two dopings. First, the room temperature electrical resistivity, ρ , increases much more strongly with doping for Ca–Th doped 123-samples than for Ca–Pr doped ones [11]. In fact, for Ca–Th doping, the depression of T_c could be qualitatively described by quantum interference effects, while for Ca–Pr doping, the depression of T_c as a function of the resistivity increase with doping was too rapid for this interpretation to be valid. In this case disorder effects are thus less prominent. A similar difference in disorder effects was inferred from the results for the thermoelectric power, which in addition indicated that instead the

localization tendency was stronger for Ca–Pr than for Ca–Th doping [12].

In the present paper we set out to investigate if differences between Ca–Th and Ca–Pr doping in the 1:2:3 compounds are manifested also in other transport properties. We have studied the Hall effect in charge neutrally doped $\text{Nd}_{1-2x}\text{Ca}_x\text{M}_x\text{Ba}_2\text{Cu}_3\text{O}_{7-\delta}$ with $\text{M} = \text{Pr}$ and Th . Experimental details are given in Section 2. In Section 3 the results are described and analyzed in two different models. The first one is a phenomenological narrow band theory, with most parameters in common with a narrow band model for the thermoelectric power [13], giving improved stability of the analyses. The second method is based on the Anderson model [14], where information on disorder and localization effects can be obtained from the temperature and concentration dependence of the parameters describing the Hall angle. These descriptions are found to be useful for analyzing data. In both cases a stronger tendency for electronic disorder with increasing doping concentration is found for Ca–Th doping, as compared to Ca–Pr doping. The results are discussed in Section 4 and briefly summarized in Section 5.

2. Experimental

Polycrystalline samples of the composition $\text{Nd}_{1-2x}\text{Ca}_x\text{M}_x\text{Ba}_2\text{Cu}_3\text{O}_{7-\delta}$ ($\text{M} = \text{Pr}$ and Th) with $0 \leq x \leq 0.10$ were prepared by standard solid state powder processing technique as described elsewhere [12]. The samples were reannealed in flowing oxygen at 460 °C for 3 days and the temperature was decreased to room temperature at a rate of 12 °C/h.

X-ray diffraction (XRD) and neutron powder diffraction have been made previously in both samples series [6,7]. The XRD results for Ca–Pr doped samples revealed a single-phase orthorhombic 123 structure for all samples. Similar results were also obtained for the Ca–Th-doped samples, except at $x = 0.10$, where a few weak impurity lines were observed [7]. This indicates that the solubility limit is somewhat below $x = 0.10$ for this doping.

Resistivity and Hall voltage measurements were made on sintered bars of typical dimensions

$0.5 \times 2.5 \times 6 \text{ mm}^3$. Electrical leads were attached to the sample by silver paint and heat treated at 300°C in flowing oxygen for half an hour, which gave contact resistances of order $1\text{--}2 \Omega$. Measurements were made using standard techniques, with four contacts for longitudinal current and voltage measurements, and additional contacts for transverse voltage measurements, including a potentiometer to compensate for any contact misalignments by nulling this voltage in zero field. Hall voltage and resistivity were measured simultaneously at each stabilized temperature by sweeping the magnetic field B in steps of 0.5 T in the sequence $0 \rightarrow +8 \text{ T} \rightarrow 0 \rightarrow -8 \text{ T} \rightarrow 0$. Thermal emfs were reduced in voltage measurements by switching current polarities. To enhance temperature stability, samples and thermometer were placed in a vacuum shield, with a weak thermal link to the surroundings. The temperature error during field sweeps was at most 0.5 K . Hall voltage measurements were made with a dc picovoltmeter with a resolution of $100\text{--}300 \text{ pV}$. The Hall voltage was linear in B for all samples and temperatures above T_c . The Hall coefficient, R_H , was calculated at each temperature from the slope of straight lines from -8 to $+8 \text{ T}$. The uncertainty in the magnitude of R_H was estimated from such fits to be less than 6% .

3. Results and analyses

Fig. 1 shows the Hall coefficient, R_H , as a function of temperature and Ca–M doping concentration in $\text{Nd}_{1-2x}\text{Ca}_x\text{M}_x\text{Ba}_2\text{Cu}_3\text{O}_{7-\delta}$ with $M = \text{Pr}$ and Th . R_H is positive in the normal state for both sample series and increases with decreasing temperature, has a maximum near $T \approx 100 \text{ K}$ and after that decreases strongly. The temperature dependence of R_H at low temperatures is stronger than that at higher temperatures. In $\text{Nd}_{1-2x}\text{Ca}_x\text{Pr}_x\text{Ba}_2\text{Cu}_3\text{O}_{7-\delta}$, R_H at high temperature did not change with x , while the peak at 100 K was slightly suppressed with increasing Ca–Pr concentration. On the other hand, for Ca–Th-doped Nd-123, R_H increased with increasing doping concentration in the whole temperature range from T_c up to room temperature. As can be seen in Fig. 1 at $x = 0$ in the Ca–Th doped series, the values for

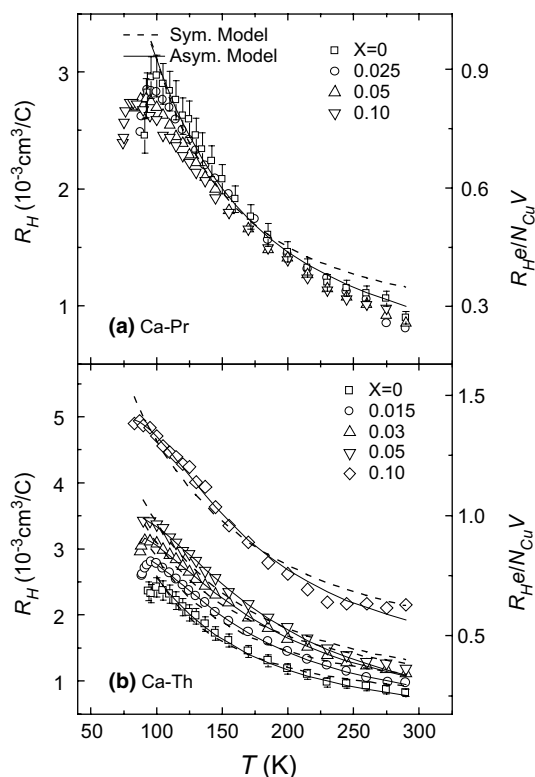


Fig. 1. The temperature dependence of the Hall coefficient R_H , for $\text{Nd}_{1-2x}\text{Ca}_x\text{M}_x\text{Ba}_2\text{Cu}_3\text{O}_{7-\delta}$ with (a) $M = \text{Pr}$ and (b) $M = \text{Th}$. The dashed and solid curves are fits to Eq. (3) in the case of symmetric and asymmetric band models, respectively. The right hand side scale shows R_H normalized to the number of Cu atoms. The bars illustrate typical estimated errors of R_H for $\text{NdBa}_2\text{Cu}_3\text{O}_{7-\delta}$.

R_H are somewhat smaller than in the Ca–Pr series. This is likely due to slightly different oxygen content and hole concentration, as found from neutron diffraction data by Rietveld refinements and bond valence sum calculations for both series [6,7]. The dashed and solid curves through data in Fig. 1 are fits to the phenomenological narrow band model in the case of symmetric and asymmetric band models, respectively, which will be described below. A fictitious hole density per Cu can be obtained from the inverse of the parameter $R_H e/N_{\text{Cu}} V$ [15]. Here N_{Cu} is the number of copper atoms in volume V . $R_H e/N_{\text{Cu}} V$ is shown by the right hand side scale in Fig. 1 as obtained from 3 Cu atoms per unit cell, and neglecting the small temperature and sample dependence of V . These

results support a decrease of the hole concentration with increasing Ca–Th doping. In comparison with charge doping, the variation in Fig. 1 is small, as can be seen e.g. from the strong increase of $R_H e/N_{Cu} V$ with reduced oxygen concentration in Y-123 [16].

The doping concentration dependence of R_H at 275 K is compared in Fig. 2 for both charge neutral doping series. R_H (275 K) is roughly constant for Ca–Pr doping, while for Ca–Th doping there is a significant increase. According to a simple one band relation between R_H and charge concentration, these changes are consistent with a decreasing charge concentration for Ca–Th and a constant charge concentration for Ca–Pr doping. From these results one may conclude that there is a more pronounced weakening of the metallic state for Ca–Th. This is qualitatively in agreement with the variation of the normal state electrical resistivity [11] and thermoelectric power [12] as a function of Ca–Pr and Ca–Th doping concentration.

Several models have been proposed to describe the Hall effect, e.g. a temperature-dependent charge carrier density [17], magnetic skew scattering [18,19], Anderson–Luttinger-liquid model [14] and a model based on paired bipolarons [20]. A phenomenological narrow band model of the electronic band structure of high- T_c superconductors has also been introduced for a wide range of dop-

ing [21], which in addition to electronic transport properties also has been used to describe the magnetic susceptibility, and the metal-insulator transition [13,21–23].

Present focus is on possible disorder effects. We have selected two models where an interpretation in such terms is possible. Our results have been analyzed in the phenomenological narrow band model [13] and in the Anderson model [14]. Although these models are apparently completely unrelated to each other, they both describe the Hall effect with parameters which are related to disorder.

3.1. Phenomenological narrow band model

In the phenomenological narrow band model [13], it was shown that all features of the resistivity $\rho(T)$, the thermoelectric power $S(T)$, and $R_H(T)$ for the Y-123 system in the normal state could be described quantitatively in a band model that supposes the existence of a narrow peak in the electronic density of states close to the Fermi level. This model contains three main parameters for $\rho(T)$ and $S(T)$ and an additional one for $R_H(T)$; the band filling by electrons F (which is equal to the ratio of number of electrons, n , to the total number of states in the band, N), the total effective bandwidth W_D in the density of states $D(E)$, and the longitudinal and transverse conductivity effective bandwidths W_σ and $W_{\sigma H}$ in the longitudinal conductivity $\sigma(E)$ and transverse conductivity $\sigma_H(E)$, respectively. Using rectangular approximations for $D(E)$, $\sigma(E)$, and $\sigma_H(E)$, motivated by the narrowness of the band, the expressions for main transport properties i.e. $\rho(T)$, $S(T)$, and $R_H(T)$ can be written as

$$\rho = \frac{1}{\langle \sigma \rangle} \frac{1 + z^{-2} + 2z^{-1} \cosh W_\sigma^*}{z^{-1} \sinh W_\sigma^*} \quad (1)$$

$$S = -\frac{k_B}{e} \left\{ \frac{W_\sigma^*}{\sinh W_\sigma^*} \left[e^{-\mu^*} + \cosh W_\sigma^* - \frac{1}{W_\sigma^*} (\cosh \mu^* + \cosh W_\sigma^*) \ln \frac{e^{\mu^*} + e^{W_\sigma^*}}{e^{\mu^*} + e^{-W_\sigma^*}} \right] - \mu^* \right\} \quad (2)$$

$$R_H = \frac{\langle \sigma_H \rangle}{\langle \sigma \rangle^2} \frac{(z-1)(v-1)^2(1+zu)^2(z+u)^2}{z(1+z)(z+v)(1+zv)(u^2-1)^2} \quad (3)$$

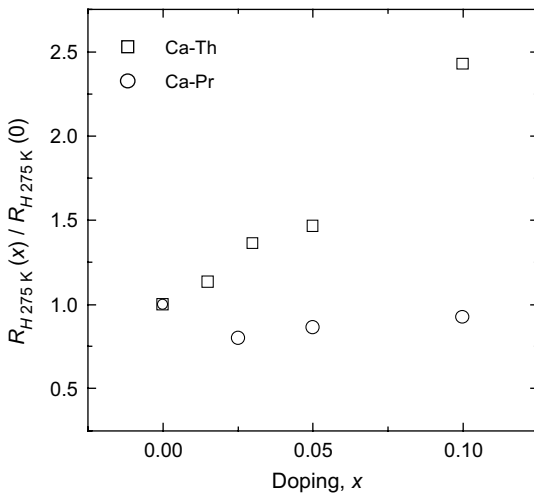


Fig. 2. The doping concentration dependence of R_H at 275 K for $Nd_{1-2x}Ca_xM_xBa_2Cu_3O_{7-\delta}$ with $M = Pr$ and Th .

$$\mu^* = \frac{\mu}{k_B T} = \ln \frac{\sinh(FW_D^*)}{\sinh[(1-F)W_D^*]} \quad (4)$$

Here $W_D^* = W_D/(2k_B T)$, $W_\sigma^* = W_\sigma/(2k_B T)$, $W_{\sigma H}^* = W_{\sigma H}/(2k_B T)$, $z = \exp(\mu^*)$, $v = \exp(W_{\sigma H}^*)$, and $u = \exp(W_\sigma^*)$. μ is the electron chemical potential and k_B the Boltzmann constant. $\langle \sigma \rangle$ and $\langle \sigma_H \rangle$ are the averages of the longitudinal and transverse (Hall) conductivity in the intervals W_σ and $W_{\sigma H}$, respectively.

We have analyzed our $R_H(T)$ data according to Eq. (3) using band width parameters inferred from fits of Eq. (2) to thermoelectric power data [12]. The results are shown by the dashed curves in Fig. 1. As can be seen there are deviations at high temperature. These deviations will be discussed below. The transverse conductivity effective bandwidth $W_{\sigma H}$ obtained from the analyses is shown in Table 1. Data for other bandwidths and the band filling fraction F have also been included in Table 1. All bandwidths (W_D , W_σ , and $W_{\sigma H}$) increase with increasing doping concentration x for both dopings. It was shown [13,24–28] that the bandwidths in this model depend on the hole concentration. When the hole concentration decreased by oxygen reduction [13] and by substitution of La on the Ba site in Y-123 [28], the bandwidth parameters increased, and with increasing hole concentration these parameters changed in the opposite way [25].

As can be seen in Table 1, the F value is almost constant for the Ca–Pr doping and increases

slightly for increasing Ca–Th doping. These results support that charge filling in the bands remains roughly constant for both series.

In order to further test the model, Eq. (1) was also fitted to resistivity data by parameters that were obtained from $S(T)$ data (see Table 1). Fig. 3 shows the resistivity data for the Ca–Th sample series in the normal state. The dashed curves through data in Fig. 3 exemplify results for one sample series. As can be seen there are strong deviations at both low and high temperature. Furthermore, the deviations increased with increasing doping concentration and the fits are rather poor for both series of samples.

It was found that a slight band asymmetry has a pronounced influence on the temperature dependence of transport properties [13,26,27]. An asymmetric band was modeled with the assumption that the center of the rectangular approximation of $D(E)$, on the one hand, and the center of $\sigma(E)$ or $\sigma_H(E)$ on the other hand, do not coincide [13] and are separated a distance bW_D . As further illustrated in the inset of Fig. 4, such an asymmetry may occur from additional states in the conduction band. With this method the expressions for $\rho(T)$, $S(T)$, and $R_H(T)$, i.e. Eqs. (1)–(3) are still valid with μ replaced by $\mu - bW_D$. To achieve good quantitative agreement between experimental results and model calculations of $R_H(T)$ and $\rho(T)$, the asymmetric phenomenological narrow band model has been used. The solid curves through

Table 1

Bandwidth parameters (W_D , W_σ , and $W_{\sigma H}$), band filling degree F of Eqs. (2) and (3), and superconducting transition temperature T_c

X	W_D (meV)	W_σ (meV)	$W_{\sigma H}$ (meV)	$F = n/N$	$c = W_D/W_\sigma$	T_c (K)
<i>Nd_{1-2x}Ca_xPr_xBa₂Cu₃O_{7-δ}</i>						
0	111(2)	33(1)	27(1)	0.519(1)	3.338(2)	91.9
0.025	150(3)	36(1)	35(1)	0.519(1)	4.233(1)	87.9
0.05	165(2)	35(1)	37(2)	0.519(2)	4.755(2)	83.2
0.10	182(3)	34(2)	43(1)	0.520(1)	5.302(3)	74.9
<i>Nd_{1-2x}Ca_xTh_xBa₂Cu₃O_{7-δ}</i>						
0	110(2)	33(1)	23(1)	0.513(2)	3.379(1)	93.6
0.015	121(2)	35(1)	32(2)	0.520(1)	3.522(2)	90.2
0.03	140(3)	37(2)	39(1)	0.527(2)	3.831(1)	86.7
0.05	159(2)	38(2)	40(2)	0.529(1)	4.228(2)	81.4
0.10	139(3)	35(2)	43(2)	0.526(2)	3.930(3)	73.2

The numbers in the parentheses are the estimated standard deviation in the last digit. All data except for $W_{\sigma H}$ were taken from Ref. [12].

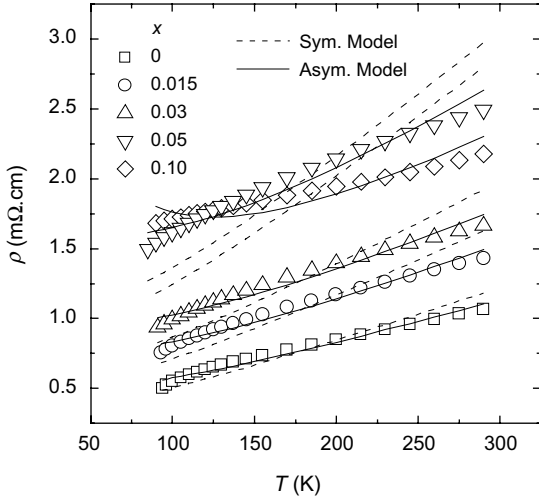


Fig. 3. Normal state resistivity as a function of temperature and doping concentration in $\text{Nd}_{1-2x}\text{Ca}_x\text{Th}_xBa_2\text{Cu}_3\text{O}_{7-\delta}$. The dashed and solid curves are fits to the model of Eq. (1) in the case of symmetric and asymmetric band models, respectively. For the asymmetric model the additional parameter b was taken from the results for R_H (Fig. 1).

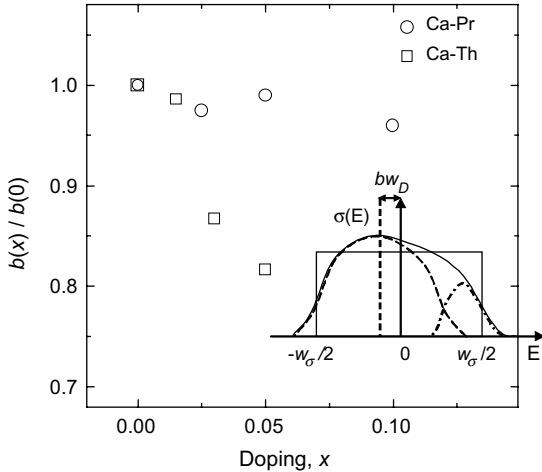


Fig. 4. Relative concentration dependence of the asymmetric parameter b for $\text{Nd}_{1-2x}\text{Ca}_x\text{M}_xBa_2\text{Cu}_3\text{O}_{7-\delta}$ with $M = \text{Pr}$ and Th . Inset: Schematic electrical conductivity $\sigma(E)$ (solid curve). The dashed and dash-dot curves show the symmetric band and the contribution of the additional states, respectively. The rectangle illustrates the model approximation of Ref. [13].

sample data in Fig. 1 and the resistivity data in Fig. 3 exemplify the fits to Ca–Th samples. As can be seen in Figs. 1 and 3, a more reliable

description is obtained on the basis of the asymmetric model. This result suggests that the band of the pure sample is also asymmetric. For the pure samples we found $b(0) = 0.072 \pm 0.005$. The relative doping concentration dependence of the asymmetry parameter b is compared in Fig. 4 for Ca–Pr and Ca–Th doping. The relative b decreased markedly with increasing x in Ca–Th doping, while for Ca–Pr doping there is at most a slight decrease. The model parameters were obtained by non-linear least square fits, and reduced chi-square values, χ^2 , were calculated.¹ For $\text{Nd}_{1-2x}\text{Ca}_x\text{Th}_xBa_2\text{Cu}_3\text{O}_{7-\delta}$, χ^2 for the symmetric model was 1.8, 2.1, 2.4, 6.3, and 9, while χ^2 for the asymmetric model was 1.2, 1.35, 1.5, 1.67, and 1.9, for $x = 0, 0.015, 0.03, 0.05$, and 0.1 respectively. These values indicate a moderately good fit for the asymmetric model with $\chi^2 \approx 1$, and a fairly poor quality of the fit for the symmetric model.

3.2. Anderson model

In the Anderson theory [14] based on Luttinger liquid ideas, spinons and holons have different relaxation mechanisms in the CuO_2 planes. Longitudinal (transport) relaxation times follow a linear T^{-1} dependence and transverse (Hall) relaxation times, follow a $\sim T^{-2}$ dependence. The longitudinal contribution gives the well-known linear- T resistivity ρ while the transverse one gives the temperature dependence of the Hall angle $\cot \theta_H \sim T^2$. In particular [14]

$$\cot \theta_H = \rho/R_H B = \alpha T^2 + \beta, \quad (5)$$

where α and β are constants. Chien et al. [29] derived the following relation from Anderson theory:

$$\alpha = \frac{k_B^2 h n}{e B W_s^2}. \quad (6)$$

where $n = k_F^2/2\pi$ is the carrier density, B the applied magnetic field, h is Planck's constant, and

¹ $\chi^2 = \frac{1}{n-d} \sum_{i=1}^n [(R_{H,im} - R_{H,io})/\sigma_{R,i}]^2$, $\sigma_{R,i}^2 = \sum_{i=1}^n [(R_{H,im} - R_{H,io})^2/(n-d)]$. $R_{H,im}$ is the measured Hall coefficient and $R_{H,io}$ is the corresponding Hall coefficient calculated from model. n is the total number of experimental points used in the fitting, d is the number of adjustable parameters, and $\sigma_{R,i}$ is the standard deviation in each experimental point.

W_s the spinon bandwidth, which is proportional to the superexchange J .

It was found in various cuprate superconductors that the results for $\cot\theta_H$ are in broad agreement with Eq. (5). In some cases deviations from this law were reported at both low and high temperatures [19,30]. The deviation at low temperature may be caused by the opening of a pseudogap in the density of states [30], while the origin of the anomaly at high temperatures is not clear.

Fig. 5 shows $\cot\theta_H$ versus T^2 calculated in magnetic field, $B = 8$ T from $\rho(T)$ and $R_H(T)$ results. It can be seen that irrespective of the complicated temperature dependencies of ρ and R_H , a quadratic-like temperature dependence of $\cot\theta_H \sim T^2$

is obtained for all x values in $\text{Nd}_{1-2x}\text{Ca}_x\text{Pr}_x\text{-Ba}_2\text{Cu}_3\text{O}_{7-\delta}$ samples. It is clear from Fig. 5b that for the samples with $x > 0$ the quadratic-like temperature dependence of $\cot\theta_H$ holds up to a temperature T_0 , which has been marked by arrows, and then starts to deviate strongly in all the Ca–Th doped samples. The deviation temperature T_0 depends on doping concentration and decreases with increasing doping concentration (Fig. 5b). The origin of this observation is not known.

From the results in Fig. 5 one finds α and β of Eq. (5). The doping dependence of α and β for both dopings is shown in Fig. 6. At $x = 0.10$, above the solid solubility limit for Ca–Th, a low value of α and β were found (not shown in

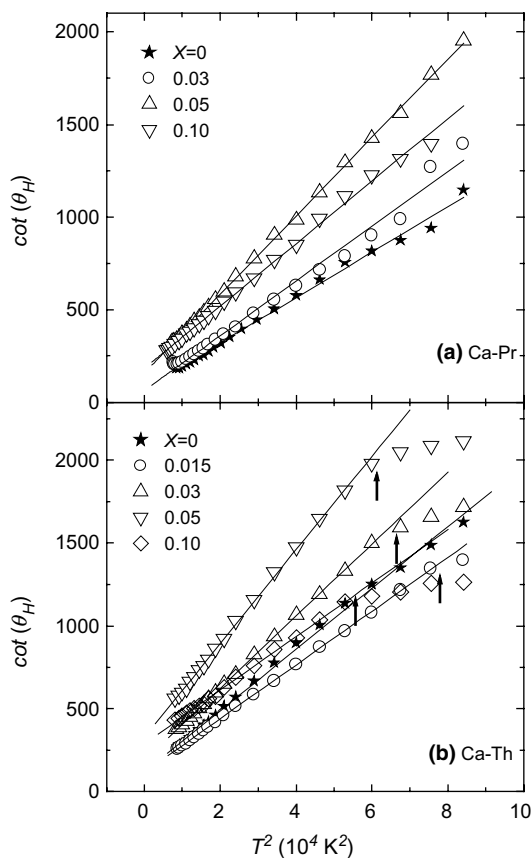


Fig. 5. (a) T^2 dependence of $\cot\theta_H = \rho/BR_H$ in $B = 8$ T for $\text{Nd}_{1-2x}\text{Ca}_x\text{M}_x\text{Ba}_2\text{Cu}_3\text{O}_{7-\delta}$ with (a) $M = \text{Pr}$ and (b) $M = \text{Th}$ as a function of doping concentration x . The solid lines in both panels are fits to Eq. (5). The deviation temperature from T^2 dependence of $\cot\theta_H$ in (b) is shown by arrows.

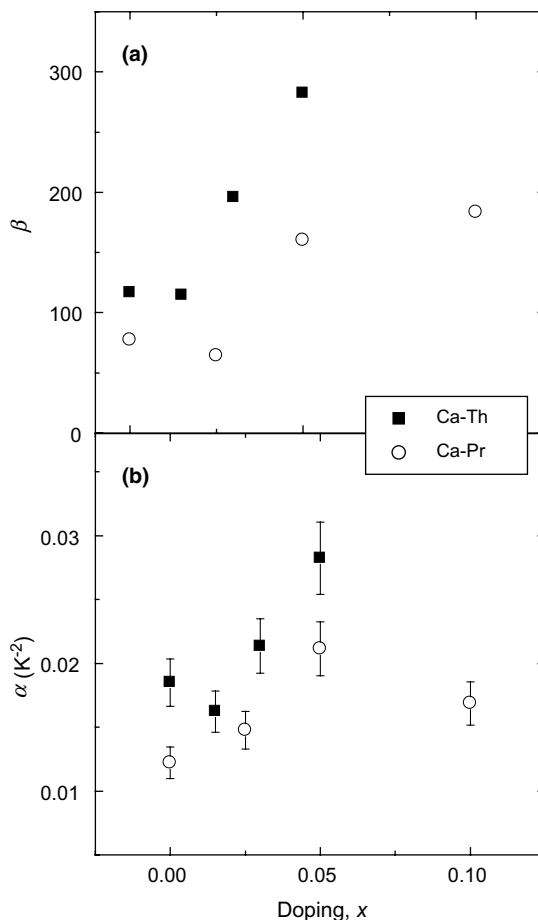


Fig. 6. Doping dependence of (a) β and (b) α in Eq. (3) for $\text{Nd}_{1-2x}\text{Ca}_x\text{M}_x\text{Ba}_2\text{Cu}_3\text{O}_{7-\delta}$ ($M = \text{Pr}, \text{Th}$). The bars illustrate typical estimated errors of α .

Fig. 6). β increases with doping in both alloys, while changes in α are fairly small. Increased β can be ascribed to increased disorder in the CuO_2 planes [23,29]. A possible small increase in α may correspond to a decrease in spinon bandwidth W_s (see Eq. (6)) since n is constant in charge neutrally doped alloys.

4. Discussion

4.1. Comparison between models

The two different models used to analyze $R_H(x, T)$ are based on different assumptions and are therefore in general difficult to compare quantitatively. However, as mentioned, β in the Anderson model and the parameter $c = W_D/W_\sigma$ in the phenomenological narrow band model both depend on disorder. Here it was found that the increase of W_D is stronger than the change of W_σ , and c increases with increased doping concentration in both alloy series (Table 1). When the solubility limit has been reached in the Ca–Th series at $x = 0.10$ [12] this trend is broken. These results for both β and c suggest a tendency for electronic disorder and localization with increased doping concentration. It was also shown that β increases linearly with increasing doping x in $\text{Y}_{1-x}\text{Ca}_x\text{Ba}_2\text{Cu}_3\text{O}_{7-\delta}$ thin films [31], in $\text{YBa}_2\text{Cu}_{3-x}\text{Zn}_x\text{O}_{7-\delta}$ single-crystals [29], and in $\text{Nd}_{1-x}\text{Ca}_x\text{Ba}_2\text{Cu}_3\text{O}_{7-\delta}$ [32], which can be ascribed to the creation of disorder in the CuO_2 plane by doping.

The band filling factor F in the phenomenological narrow band model corresponds qualitatively to the α parameter in the Anderson model. According to the definition of F and Eq. (6), both parameters depend on charge carrier density. As can be seen from Table 1 and Fig. 6, the variation with doping of both parameters is limited, and within 0.52 ± 0.01 and 0.02 ± 0.01 for F and α , respectively. This is in agreement with expectations for charge neutral dopings.

The strong depression rate in charge neutral dopings, $-dT_c/dx \approx 200$ K for $\text{Nd}_{1-2x}\text{Ca}_x\text{M}_x\text{Ba}_2\text{Cu}_3\text{O}_{7-\delta}$ with $M = \text{Pr}$ and Th [6,7,12], is an interesting effect. Fig. 7 shows the relation between the superconducting critical temperature T_c and

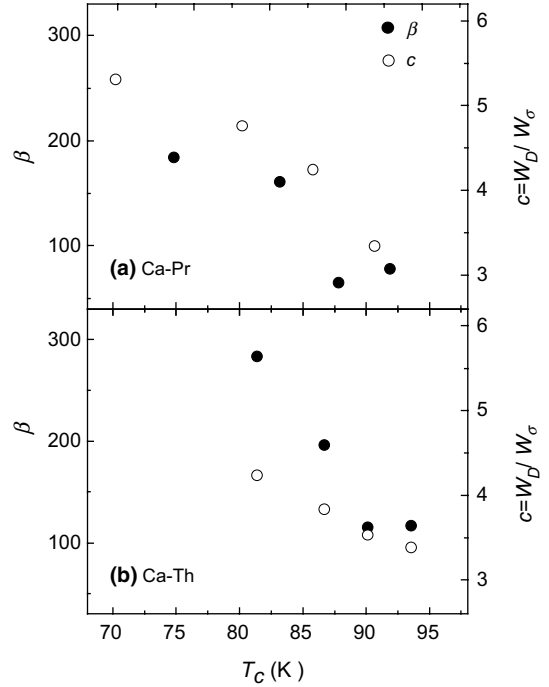


Fig. 7. β versus critical temperature T_c for $\text{Nd}_{1-2x}\text{Ca}_x\text{M}_x\text{Ba}_2\text{Cu}_3\text{O}_{7-\delta}$ with (a) $M = \text{Pr}$ and (b) $M = \text{Th}$ from the Anderson model (left hand scale). $c = W_D/W_\sigma$ as a function of T_c for $\text{Nd}_{1-2x}\text{Ca}_x\text{M}_x\text{Ba}_2\text{Cu}_3\text{O}_{7-\delta}$ with (a) $M = \text{Pr}$ and (b) $M = \text{Th}$ from the phenomenological narrow band model (right hand scale).

the temperature independent constant β on one hand and the tendency for localization c on the other hand. Both β and c increase linearly as T_c decreases by increased doping concentrations. Therefore, these results support that both Ca–Pr and Ca–Th introduce disorder, which enhances the localization tendency of mobile holes in the CuO_2 plane. Thus the depression of T_c can be qualitatively explained in the picture of electronic disorder.

4.2. Differences between Ca–Th and Ca–Pr

It is useful to summarize various properties of Ca–Th and Ca–Pr doped Nd-123 in light of results from R_H . Although these dopings in several aspects are similar, there are noteworthy differences as mentioned in Section 1. Two of the most significant differences in transports properties are the

stronger increase of the room temperature electrical resistivity ρ and the thermoelectric power S for Ca–Th doped samples, as compared to Ca–Pr doped samples [12]. Another interesting difference is shown in Fig. 1 where R_H (275 K) increases strongly in the Ca–Th case while it is roughly constant for the Ca–Pr series. The present result for R_H is also in line with the doping dependence of the room temperature ρ and S .

Another interesting feature is the variation with doping of the relative conduction band asymmetry parameter in the phenomenological narrow band model. As can be seen from Fig. 4, the relative decrease of the conduction band asymmetry parameter b with x is much stronger for Ca–Th than Ca–Pr doping. On the other hand, it was shown that b is related to the total number of states in the conduction band N , with an increase of b for increasing additional states [26]. Therefore, our results indicate that an increase in x leads to a stronger decrease in the number of states N for Ca–Th doping than for Ca–Pr doping. Furthermore, an increased $F = n/N$ with Ca–Th doping (Table 1) supported a decrease in the number of states since the electron density n is constant for charge neutral doping. Thus, from these results it can be concluded that a decrease of the parameter b supports an increased localization tendency for both dopings which is stronger for Ca–Th than for Ca–Pr doping.

5. Brief conclusion

The transport properties of sintered samples of $\text{Nd}_{1-2x}\text{Ca}_x\text{M}_x\text{Ba}_2\text{Cu}_3\text{O}_{7-\delta}$ with $M = \text{Pr}$ and Th have been studied in the normal state. A phenomenological narrow band model could well describe the results for the Hall coefficient and the thermoelectric power. On the basis of this model, it was found that the conduction bandwidths increased with doping concentration for both dopings and the band filling of electrons was roughly constant for Ca–Pr doping while it increased with Ca–Th. It was also found that the conduction band was asymmetric for undoped samples and that the degree of asymmetry decreased with increasing Ca–Th doping, and was almost constant for

Ca–Pr doped alloys. In the view of the Anderson model, the temperature dependent part of the Hall angle was roughly proportional to T^2 for Ca–Pr in the whole measured temperature range while a deviation was observed from this behavior at high temperature for Ca–Th doping. The results of both models suggest that Ca–Pr and Ca–Th introduce electronic disorder which drives a tendency of localization of mobile holes in the CuO_2 -plane. This result was obtained in two widely different models for the Hall coefficient, which strengthens the conclusion of a disorder effect. We can conclude that disorder effects in charge neutrally doped 123 compounds appear to be firmly manifested in the normal state electronic transport properties of these compounds, including the resistivity, the thermoelectric power as well as the Hall effect.

Acknowledgments

Financial support by the Tarbiat Moallem University of Sabzevar, the Swedish Research Agency Vetenskapsrådet (VR), and the Swedish OXIDE Programme are gratefully acknowledged.

References

- [1] J.L. Tallon, C. Bernhard, H. Shaked, R.L. Hitterman, D.J. Jorgensen, Phys. Rev. B 51 (1995) 122.
- [2] J.J. Neumeier, T. Bjørnholm, M.B. Maple, I.K. Schuller, Phys. Rev. Lett. 63 (1989) 2516.
- [3] M. Andersson, Z. Hegedüs, M. Nygren, Ö. Rapp, Physica C 160 (1989) 65.
- [4] M. Andersson, Ö. Rapp, T.L. Wen, Z. Hegedüs, M. Nygren, Phys. Rev. B 48 (1993) 7590.
- [5] T.C. Poon, J.C. Gao, Physica C 256 (1996) 161.
- [6] P. Lundqvist, C. Tengroth, Ö. Rapp, R. Tellgren, Z. Hegedüs, Physica C 269 (1996) 231.
- [7] P. Lundqvist, Ö. Rapp, R. Tellgren, I. Bryntse, Phys. Rev. B 56 (1997) 2824.
- [8] H. Iwasaki, J.-I. Sugawara, N. Kobayashi, Physica C 185–189 (1991) 1249.
- [9] A. Okada, J. Arai, U. Umezawa, Physica C 235–240 (1994) 817.
- [10] S.R. Ghorbani, M. Andersson, Ö. Rapp, Phys. Rev. B 69 (2004) 14503.
- [11] B. Lundqvist, P. Lundqvist, Ö. Rapp, Phys. Rev. B 57 (1998) 14428.
- [12] S.R. Ghorbani, M. Andersson, Ö. Rapp, Phys. Rev. B 66 (2002) 104519.

- [13] V.E. Gasumyants, V.I. Kaidanov, E.V. Vladimirskaia, *Physica C* 248 (1995) 255.
- [14] P.W. Anderson, *Phys. Rev. Lett.* 67 (1991) 2092.
- [15] J.R. Copper, J.W. Loram, *J. Phys. I* 6 (1996) 2237.
- [16] Y. Ando, Y. Hanaki, S. Ono, T. Murayama, K. Segawa, N. Miyamoto, S. Komiya, *Phys. Rev. B* 61 (2000) R14956.
- [17] Y. Kubo, T. Kondo, Y. Shimakawa, T. Manako, H. Igarashi, *Phys. Rev. B* 45 (1992) 5553.
- [18] A.T. Fiory, G.S. Grader, *Phys. Rev. B* 38 (1988) 9198.
- [19] B. Wuyts, V.V. Moshchalkov, Y. Bruynseraede, *Phys. Rev. B* 53 (1996) 9418.
- [20] A.S. Alexandrov, V.N. Zavaritsky, S. Dzhumanov, *Phys. Rev. B* 69 (2004) 052505.
- [21] V.V. Moshchalkov, *Physica C* 156 (1988) 473.
- [22] V.V. Moshchalkov, *Physica B* 163 (1990) 59.
- [23] C. Quitmann, D. Andrich, C. Jarchow, M. Fleuster, B. Beschoten, G. Güntherodt, V.V. Moshchalkov, G. Mante, R. Manzke, *Phys. Rev. B* 46 (1992) 11813.
- [24] V.E. Gasumyants, V.V. Valadimirskaia, M.V. Elizarova, N.V. Ageev, *Phys. Solid State* 40 (1998) 1943.
- [25] V.V. Valadimirskaia, V.E. Gasumyants, I.B. Patarina, *Phys. Solid State* 37 (1995) 1084.
- [26] V.E. Gasumyants, M.V. Elizarova, I.B. Patarina, *Supercond. Sci. Technol.* 13 (2000) 1600.
- [27] N.V. Ageev, V.E. Gasumyants, V.I. Kaidanov, *Phys. Solid State* 37 (1995) 1171.
- [28] V.E. Gasumyants, E.V. Valadimirskaia, I.B. Patarina, *Phys. Solid State* 40 (1998) 14.
- [29] T.R. Chien, Z.Z. Wang, N.P. Ong, *Phys. Rev. Lett.* 67 (1991) 2088.
- [30] Y. Abe, K. Segawa, Y. Ando, *Phys. Rev. B* 60 (1999) R15055.
- [31] H. Yakabe, I. Terasaki, M. Kosuge, Y. Shiohara, N. Koshizuka, *Phys. Rev. B* 54 (1996) 14986.
- [32] S.R. Ghorbani, M. Andersson, Ö. Rapp, *Physica C* 390 (2003) 161.